MOLECULAR BIOLOGY

Human telomere length is chromosome end–specific and conserved across individuals

Kayarash Karimian[1,2], Aljona Groot[3], Vienna Huso[1,2], Ramin Kahidi[4], Kar-Tong Tan[5,6,7], Samantha Sholes[1,2]†, Rebecca Keener[2,8], John F. McDyer[9], Jonathan K. Alder[9], Heng Li[10,11], Andreas Rechtsteiner[3], Carol W. Greider[1,3]*

Short telomeres cause age-related disease, and long telomeres contribute to cancer; however, the mechanisms regulating telomere length are unclear. We developed a nanopore-based method, which we call Telomere Profiling, to determine telomere length at nearly single-nucleotide resolution. Mapping telomere reads to chromosome ends showed chromosome end–specific length distributions that could differ by more than six kilobases. Examination of telomere lengths in 147 individuals revealed that certain chromosome ends were consistently longer or shorter. The same rank order was found in newborn cord blood, suggesting that telomere length is determined at birth and that chromosome end–specific telomere length differences are maintained as telomeres shorten with age. Telomere Profiling makes precision investigation of telomere length widely accessible for laboratory, clinical, and drug discovery efforts and will allow deeper insights into telomere biology.

Human health is profoundly affected by telomere length, yet the detailed mechanism of length regulation is poorly understood. Telomeres are maintained around an equilibrium distribution with constant shortening at each round of DNA replication, counterbalanced by de novo addition of telomere sequence repeats by telomerase (*1*). Failure to maintain the length distribution leads to inherited short telomere syndromes that manifest as age-related degenerative diseases such as pulmonary fibrosis, immunodeficiency, and bone marrow failure (*2*). Conversely, long telomeres predispose individuals to cancer (*3*), and mutations that increase telomerase expression are one of the most common in cancer (*4*, *5*). However, lack of widely accessible and accurate methods for measuring telomere length has limited development of targeted therapies.

Precisely how telomerase action maintains a length equilibrium is of great interest. Telomerase stochastically elongates short telomeres more frequently than long telomeres (*6*), supporting the "protein counting" model for the length maintenance (*7*, *8*), which suggests that proteins bound along TTAGGG repeats negatively regulate telomere elongation in cis. In this model, the telomere length equilibrium is maintained by specifically lengthening shorter telomeres to precisely counterbalance shortening of all telomeres. An implication of this model is that all telomeres will be regulated around a similar mean length distribution.

Telomere length distribution was first identified using Southern blotting, which revealed a Gaussian-like distribution of telomere lengths (*9*, *10*). As this method reports on all telomeres in the cell, the protein counting model was proposed to account for the length distribution across all telomeres (*11*–*13*). Similarly, the FlowFISH (flow cytometry fluorescence in situ hybridization) assay (*14*) used for diagnosis of telomere-related diseases (*15*–*17*) also reports on the mean length of all telomeres in the cell. The correlation between FlowFISH measurements and disease could imply that mean telomere length is the biologically relevant measurement, when in fact it might not be. Instead, the global mean may correlate with a different variable, such as chromosome-specific telomere lengths, as we describe here.

Other methods, such as qFISH (quantitative fluorescent in situ hybridization), allow measurement of individual telomeres in metaphase spreads (*18*) and have suggested that telomeres on all chromosome arms are not globally regulated around a common length distribution (*19*–*21*). However, FlowFISH and qFISH are highly specialized methods and are not widely used. Here we present Telomere Profiling, a reproducible, accurate, and accessible tool that measures the length of each individual telomere in the cell at near-nucleotide resolution. We establish that individual telomeres on specific chromosome ends are indeed maintained around distinct length distributions. The advantages of Telomere Profiling in telomere analysis will enable exploration of entirely new areas of telomere biology.

Results

We developed the Telomere Profiling method to physically enrich and sequence telomeres using Oxford Nanopore Technologies (ONT) MinION long-read sequencing. We digested the DNA, then ligated telomeric ends with a biotinylated oligonucleotide (TeloTag), and isolated the tagged telomeres with streptavidin. We released telomeres by restriction enzyme digestion and sequenced them using the MinION (Fig. 1A). Telomere profiling resulted in an ~3400-fold increase in telomere reads compared to whole genome sequencing (Fig. 1C and see methods in the supplementary materials). Multiplexing samples generated ~50,000 telomere reads per flow cell, with an average fragment length (subtelomere + telomere) of ~20 kb. The method is affordable, with a cost per sample when multiplexing of ~$80 to $140 (see methods). To establish whether nanopore sequencing accurately determines the length of telomeric repeats, we sequenced a plasmid with an ~500–base pair (bp) $(TTAGGG)_n$ insert. The median length of the TTAGGG sequence was 501 bp with a 95% confidence interval of ±1 bp (fig. S1, D and E), highlighting the accuracy of length determination.

Bioinformatic analysis of telomere length

We determined both "bulk length" (all telomeres) and chromosome end–specific lengths bioinformatically. We used ONT Guppy software for basecalling and then filtered for telomere reads (see methods). We initially determined telomere length by mapping (*22*–*25*) reads to a custom reference genome and determined the number of nucleotides from subtelomere to the TeloTag (see methods). This method is robust when the sequence reads and reference genome are very similar. However, mapping reads from many different individuals to one reference caused errors in length determination because the subtelomere sequences vary in the population, causing over- or under-calling of telomere lengths (fig. S2). To overcome this, we developed an algorithm, TeloNP, to define the telomere length on each individual telomere read. TeloNP defines the subtelomere boundary on the basis of a discontinuity in telomere sequence content and measures length from that boundary to the TeloTag (Fig. 1B and fig. S3, A and B; see methods).

[1]Department of Molecular Biology and Genetics, Johns Hopkins University School of Medicine, Baltimore, MD, USA. [2]Biochemistry, Cellular and Molecular Biology Graduate Program, Johns Hopkins University School of Medicine, Baltimore, MD, USA. [3]Department of Molecular Cell and Developmental Biology, University of California, Santa Cruz, CA, USA. [4]Health Sciences Program, Cumming School of Medicine, University of Calgary, Calgary, AB, Canada. [5]Department of Genetics, Harvard Medical School, Boston, MA, USA. [6]Department of Medical Oncology, Dana-Farber Cancer Institute, Boston, MA, USA. [7]Cancer Program, The Broad Institute, Cambridge, MA, USA. [8]Department of Biomedical Engineering, Johns Hopkins University, Baltimore, MD, USA. [9]Pulmonary, Allergy, Critical Care, and Sleep Medicine Division, Department of Medicine, University of Pittsburgh, Pittsburgh, PA, USA. [10]Department of Data Sciences, Dana-Farber Cancer Institute, Boston, MA, USA. [11]Department of Biomedical Informatics, Harvard Medical School, Boston, MA, USA.
*Corresponding author. Email: cgreider@ucsc.edu
†Present address: Merck & Co., West Point, PA, USA.

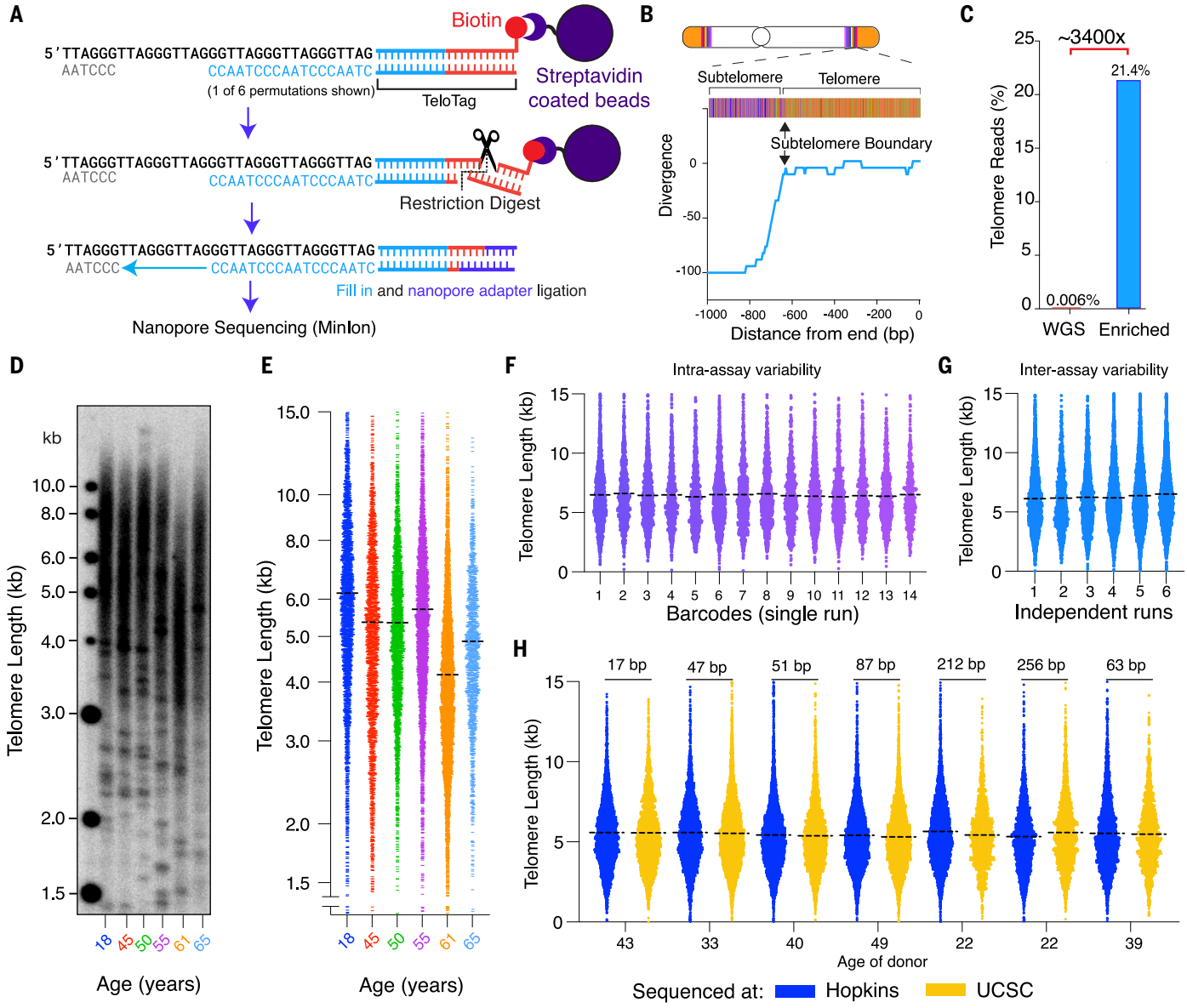

Fig. 1. Telomere Profiling is accurate and precise. (**A**) Schematic depicting the Telomere Profiling enrichment method. Telomeres are tagged with a biotin adapter (TeloTag), enriched by streptavidin pull-down, and sequenced. (**B**) Subtelomere boundary is identified using an algorithm, TeloBP, that detects substantial deviation from the telomere repeat pattern. (**C**) Comparison of Telomere Profiling versus whole genome sequencing (WGS). (**D**) Southern blot of telomere lengths from six individuals of different age. (**E**) Telomere length measured by Telomere Profiling for the same individuals as in (C) (total reads = 21,556). The dashed line represents the median telomere length of each distribution. Each point represents a single telomere read. (**F**) Intra-assay variability: Telomere length from a single donor was measured 14 times on a single flow cell (total reads = 13,256). (**G**) Interassay variability: Telomere length measured from a single donor across six different flow cells (total reads = 19,230). (**H**) Telomere length profiles from the same samples generated in two different laboratories, Johns Hopkins University (blue) and the University of California, Santa Cruz (gold). The difference in telomere length in base pairs is shown at the top.

To benchmark the length accuracy, we modified an approach (*26*) to examine the nanopore raw current signals using the algorithm TeloPeakCounter (fig. S4, A and B; see methods). Telomere length determined using Guppy basecalling was tightly correlated with the length determined by TeloPeakCounter. We therefore adopted Guppy basecalling for length determination (fig. S4, C and D).

Telomere Profiling accurately and reproducibly reports telomere length

We performed Telomere Profiling on blood or peripheral blood mononuclear cells (PBMCs) from six people ranging in age from 0 to 91 years (Fig. 1E) (see methods) and found length trends similar to those shown by Southern blot (Fig. 1D). To test reproducibility, we measured telomere length of DNA from one individual on the same flow cell (Fig. 1F and fig. S1F) [coefficient of variation (CV): 1.3%] or on different flow cells (Fig. 1G and fig. S1G) (CV: 2.4%). This low variability compares well with FlowFISH with an interassay CV of 2.2% and outperformed the frequently used quantitative polymerase chain reaction assay (interassay CV: 25.0%) (*16*). We also tested interlaboratory variability using samples enriched and sequenced

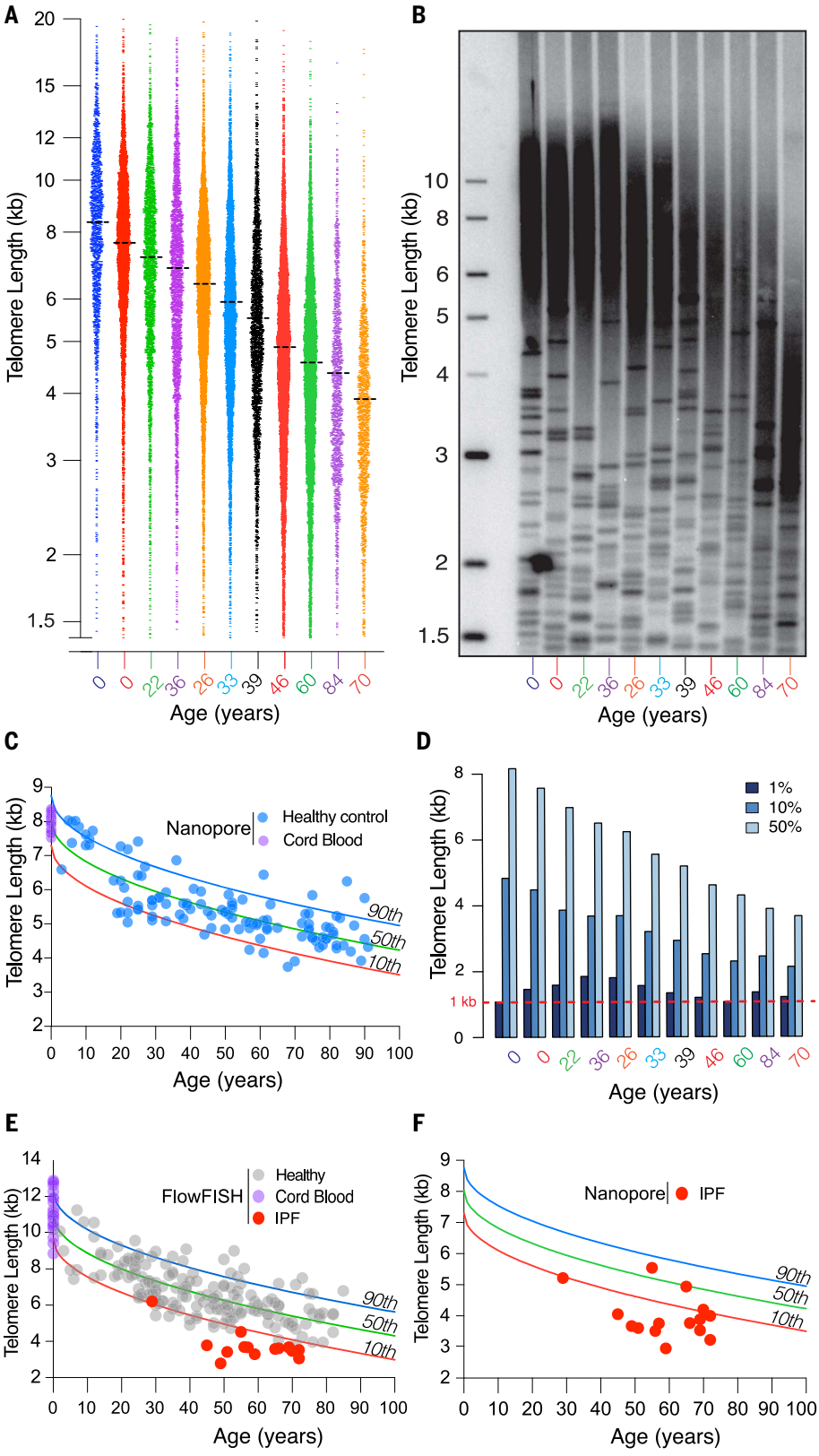

Fig. 2. Telomere Profiling measures telomere shortening with age and detects individuals with short telomere syndromes. (**A**) Telomere length profiles for 11 samples selected (age is noted at bottom). Each point is an individual read (total reads = 47,624). (**B**) Prospective Southern blot of same samples as (A). Age of individual noted at bottom. (**C**) The mean elomere length was determined for 132 individuals aged 0 to 91 (blue dots). Cord blood lengths are shown in purple. The population distribution and confidence intervals for the 90th (blue line), 50th (green line), and 10th percentiles (red line) for telomere length in this population are shown using parameters established for FlowFISH (*16*). (**D**) For each individual in (A), we examined the reads that fell into the 50th, 10th, and 1st percentiles for telomere lengths. The red dashed line indicates 1-kb telomere length. (**E**) Lymphocyte telomere length from FlowFISH data from (*16*) (gray dots); cord blood length is shown with purple dots. The lengths for 15 individuals with IPF were determined by FlowFISH (red dots). One point represents two individuals who have nearly identical length and are indistinguishable. (**F**) Nanopore telomere length profiles from the same 15 individuals with IPF are shown plotted against population distribution from (C) (total reads = 32,457).

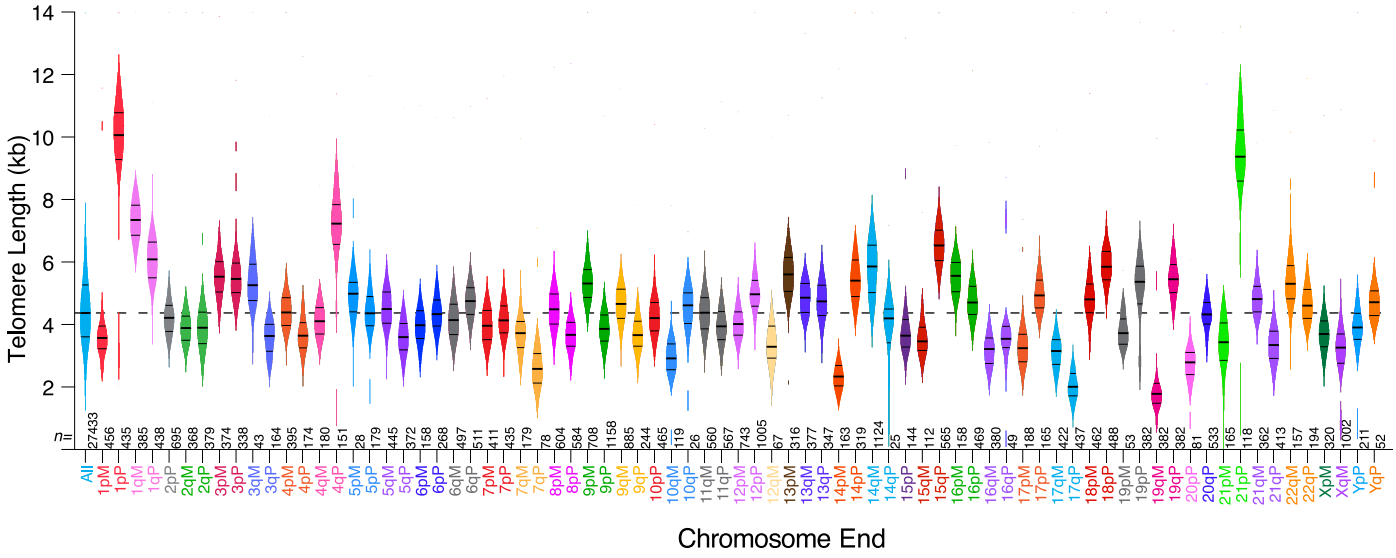

Fig. 3. Chromosome end–specific telomere lengths. Violin plots of the distribution of telomere lengths in the HG002 cell line for the ends that passed our filters. Each end is labeled with the chromosome number and "p" for the short or "q" for the long arm. The haplotypes for each chromosome end are labeled "M" for maternal or "P" for paternal and colored with the same colors for allelic pairs. The median, 1st, and 3rd quartiles for each distribution are shown with short horizontal black lines in each violin plot. The distribution of all telomere lengths across all chromosome ends is at the far left ("All"), and the dashed line represents this grand median of all telomeres. The number of reads for each chromosome end is shown at the bottom of each violin plot. Analysis of the means (ANOM) multiple contrast test of each telomere length distribution against the grand mean of all telomere lengths is shown in fig. S5D.

by different people in different labs (Fig. 1H). To determine whether DNA fragment size affects telomere length determination, we compared restriction enzyme cutting that generated ~9-kb fragments to enzymes that generated ~25-kb fragments and found similar telomere lengths (fig. S5, A and B), which indicates that fragment length in this range did not bias telomere length determination.

Telomere Profiling measures telomere shortening with age and detects individuals with short telomere syndromes

Telomere length shortens with age in PBMCs (*16*, *27*–*30*). To test the dynamic range of Telomere Profiling, we sequenced 11 individuals ranging in age from 0 to 84 (Fig. 2A) and loaded a Southern blot with the lane order ranked by nanopore lengths. The Southern blot broadly showed the same rank order as Telomere Profiling (Fig. 2, A and B). We examined the 1st, 10th, and 50th percentiles of telomere length for each sample and saw an age-dependent decrease in the 50th and 10th percentiles; however, the 1st percentile telomere length did not decrease, suggesting that there is a threshold length in PBMCs below which telomeres cannot be maintained (Fig. 2D).

We examined the population distribution for 132 donors ranging in age from 0 to 90 (Fig. 2C) and compared it to the distribution seen with FlowFISH (Fig. 2E). We defined 90th, 50th, and 10th intervals for mean telomere length using the same statistical methods used for FlowFISH (*16*). The shapes of the age-dependent curves were similar; however, the absolute lengths of the telomeres were longer with FlowFISH. Cord blood showed a mean of 7986 ± 245 bp (Fig. 2C), whereas the FlowFISH data (*16*) showed a mean of 10,980 ± 1190 (Fig. 2E). This discrepancy is likely due to normalization of FlowFISH fluorescence signal to a reference donor measured on a Southern blot. Southern telomere restriction fragments include subtelomeric sequences, which increase the apparent telomere length. Estimates of telomere lengths from Southern blots are known to vary between laboratories (*31*); likewise, FlowFISH cord blood telomere length estimates vary from ~18 kb (*32*) to ~11 kb (*16*) to ~9 kb (*33*). In contrast, Telomere Profiling reports a reproducible length that can be directly compared between laboratories (Fig. 1H).

To compare our method directly to the clinical FlowFISH assay, we sequenced archived DNA (blinded) from individuals with idiopathic pulmonary fibrosis (IPF), the most common clinical manifestation of short telomere syndrome (*34*). Telomere length determined by Telomere Profiling (Fig. 2F) in most IPF samples was similar to the FlowFISH measurement (Fig. 2E), although two samples did show different lengths, likely because archived DNA was from whole blood containing a mixture of lymphocytes and granulocytes. FlowFISH distinguishes telomere lengths in lymphocytes and granulocytes (*35*, *36*), and they are usually concordant, however in some individuals, telomere lengths differ in these two cell types (*16*, *37*, *38*). Thus, although Telomere Profiling may in the future be used as a diagnostic, additional development, such as isolation of specific cell types before sequencing, may be required.

Human telomeres have chromosome end–specific lengths

We examined telomere length at each individual chromosome end in the diploid HG002 cell line, for which a high-quality reference genome is available (*39*). Mapping to subtelomeres is a challenge because these regions consist of many paralogy blocks that share sequences among different chromosomes (*23*, *40*). Tan *et al.* found that Minimap2 (*41*, *42*) aligns reads to the correct telomere with high accuracy when there is a subtelomere sequence of 10 kb (*43*). We mapped our reads that had an average length of 16.4 kb (4.6-kb telomere repeats and 11.7-kb subtelomeric sequence) to the HG002 reference genome (see methods). Each individual chromosome end showed a distinct telomere length distribution (Fig. 3). Of the 77 chromosome ends that passed our quality filters (see methods), 66 had significant differences in length distribution compared with the grand mean (Fig. 3). In fact, some telomeres also showed significant length differences even between the maternal (M) and paternal (P) haplotypes. While the median telomere length was 4.6 kb, the telomere length of 1pM and 1pP differed by >6 kb. Discovering what regulates chromosome end–specific length differences will provide critical insight into telomere length regulation.

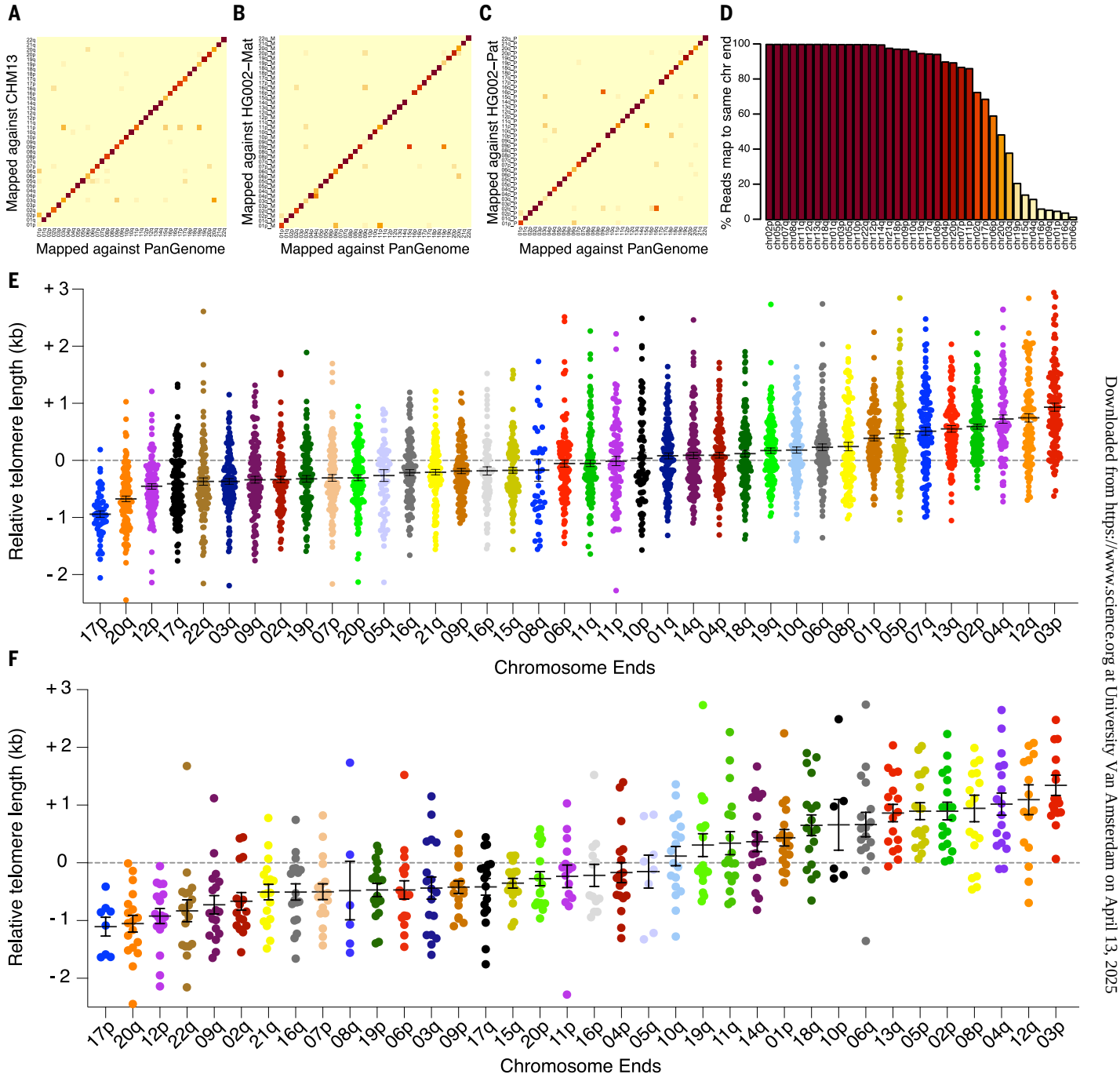

Fig. 4. Conserved chromosome-specific telomere rank order across 147 individuals. We used the pangenome reference to assign reads to chromosome ends for 147 individuals and compared where they mapped in three other references. (**A**) Matrix heatmap shows what fraction of reads mapped to a given chromosome end in the pangenome (column) and where they map in CHM13 (rows) with a mapq (mapping quality score) of 60. Light yellow indicates 0% and dark red indicates 100% of reads mapping to the respective chromosome end. (**B**) As in (A), but mapping to the HG002 maternal reference. (**C**) As in (A), but mapping to the HG002 paternal reference genome. (**D**) Bar graph showing the fraction of reads that mapped for each chromosome end in the pangenome to the same chromosome end in all three haploid genomes (CHM13, HG002 maternal, and HG002 paternal). Colors are the same as in the heatmaps. (**E**) The relative telomere length for each individual and each chromosome end was calculated. The grand mean telomere length for a given individual was subtracted from the chromosome-specific mean telomere length for each chromosome end in that individual. Zero indicates no difference between the chromosome-specific mean telomere length and the individual's grand mean telomere length. Bars represent mean length of a given telomere in all individuals, and whiskers represent the standard error of the mean. (**F**) Same as in (E), but for cord blood samples only.

Chromosome-specific telomere length differences are conserved across individuals

We examined chromosome end–specific lengths in the 147 individuals described in Fig. 2. We mapped telomere reads to the subtelomere sequences from the recently released pangenome reference from 47 high-quality Telomere-to-Telomere (T2T) assemblies (*44*) and filtered for reads with >1 kb of alignment (see methods). We removed the acrocentric and X and Y chromosome ends because the high rate of meiotic recombination at these ends does not allow them to map uniquely (*45*).

To estimate whether our pangenome analysis reproducibly mapped reads to the same subtelomere, or whether there might be mismapping, we compared where the reads mapped in the pangenome to where they mapped in three different haploid reference genomes—CHM13, HG002 maternal, and HG002 paternal—using a matrix heatmap (Fig. 4, A to C). The diagonal indicates the fraction of reads from the pangenome mapping that map to the same chromosome end in the haploid genomes. We next quantified the percent of reads that mapped to the same chromosome end in the pangenome and all three haploid reference genomes (Fig. 4D and fig. S6, A to C). For 33 of the 39 chromosome ends, 60 to 100% of the reads mapped to the same end in all three haploid genomes. As a control, we examined the acrocentric chromosomes that are expected to map to different ends in different individuals. We found that no reads from the acrocentrics mapped back to the same chromosome end in all three references (fig. S6D). This gives confidence that our filter will remove reads that map to multiple ends, increasing our confidence in the correct mapping.

To compare the telomere length of each chromosome end across the aging population, we established the relative mean telomere length. We calculated the grand mean telomere length for a given individual and subtracted it from the chromosome-specific mean telomere length for each chromosome end for that individual. Zero indicates that there is no difference between the specific chromosome end mean telomere length and the individual's grand mean telomere length (Fig. 4E). We ranked the chromosome ends by their relative telomere lengths and found that 17p, 20q, and 12p tended to be the shortest telomeres across the population, whereas 4q, 12q, and 3p tended to be the longest (Fig. 4E). Thus, although haplotype-specific differences in telomere length are seen in the HG002 cell line (Fig. 3), across a population, on average, certain chromosome ends are more likely to be shorter, while others are more likely to be longer, than the grand mean. Previous work using qFISH to measure telomere length on metaphase spreads in 10 individuals also found 17p, 20q, and 12p among the four shortest telomeres and 4q, 12q, and 3p among the eight longest telomeres (*20*), strengthening the conclusion that some chromosome ends are reproducibly shorter or longer than the grand mean.

To determine whether chromosome end–specific telomere lengths are present at birth, we mapped the reads from cord blood to the pangenome and calculated the relative mean telomere lengths as described above (Fig. 4F). We found again that 17p, 20q, and 12p were shorter, and 4q, 12q, and 3p longer, than the grand mean. This supports previous work (*46*) that suggested that differences in individual telomere lengths are established at birth.

Discussion

A fundamental understanding of the mechanisms that regulate telomere length is essential to develop future disease treatments. When the telomere length distribution shifts shorter, some telomeres become critically short, initiating senescence (*47*–*50*), and can cause age-related degenerative disease in humans (*17*). Inherited mutations that shift to a longer equilibrium predispose individuals to cancer (*3*, *51*), and the most frequent somatic mutations in cancer increase telomerase levels and lengthen telomeres (*4*, *5*). Telomere Profiling will enable the dissection of how individual telomere lengths on specific chromosomes are maintained as well as their potential role in triggering senescence and, ultimately, disease.

Chromosome end–specific telomere length equilibria imply previously unknown regulatory mechanisms

The predominant protein-counting model for telomere length maintenance proposes that telomere proteins that bind TTAGGG repeats repress the elongation of the telomere in cis (*7*, *52*) and that longer telomeres have more repression, allowing shorter telomeres to be preferentially elongated (*6*). This model represents a robust way to maintain a length equilibrium (*53*). However, given that all telomeres have the same TTAGGG repeats, the model predicts that all telomeres would be regulated around a shared equilibrium length. The demonstration of end-specific lengths indicates that other, yet unknown factors can play a key role in regulating telomere length.

In yeast that lack telomerase, all telomeres shorten at similar rates (*22*), which suggests that telomere elongation, not shortening, is the major influence on chromosome-specific lengths. Telomere elongation is the sum of the frequency of elongation of any given end (telomerase recruitment) and number of repeats added per elongation event (telomerase processivity). When the sum of these events, on average, equals the rate of telomere shortening, the equilibrium point is set. However, given end-specific length distributions, it is clear that this simple view does not represent the full complexity of the system. There must be factors at specific chromosome ends that regulate telomerase recruitment, processivity, or both to establish end-specific lengths. In addition, stochastic shortening, such as telomere rapid deletion (*54*) or replication fork collapse (*55*, *56*), may play yet unknown roles in establishing telomere length equilibrium.

Mechanisms that may influence end-specific telomere length

Subtelomeric sequences are obvious candidates to regulate end-specific telomere lengths. In yeast, subtelomere DNA binding proteins can affect telomere length (*57*), although the mechanism is not yet understood. The subtelomeric TAR1 element (*58*) present in paralogy block 23 (*25*, *40*) was proposed to regulate telomere length, possibly through binding CTCF and regulating expression of the long noncoding RNA TERRA (*59*–*61*). However, we did not find a direct relationship of the shortest telomeres in our data with the ends that lack TAR1. Future comprehensive analysis of the subtelomere sequences will lead to new testable models for establishment of telomere length equilibria.

Epigenetic modifications of DNA or histones may influence telomere length (*62*). Human and mouse subtelomeric regions are known to be methylated at CpG sites (*63*), and experiments in mice suggest that loss of DNA methyltransferases results in shorter telomeres (*64*). Subtelomere sequences may also influence other mechanisms that have been proposed to regulate telomere length, such as replication timing and tethering to the nuclear periphery (*65*). The availability of Telomere Profiling will allow exploration of the role of these factors in establishing telomere length equilibria.

Chromosome end–specific length differences are present at birth and maintained as telomeres shorten with age

Telomere length is inherited from parent to child. Evidence of this comes from the genetic anticipation in short telomere syndromes; short telomeres are passed down to each generation, and the severity of disease increases across generations (*66*). Similarly, in mice heterozygous for telomerase deletion, progressively shorter telomeres are passed down across six generations, causing progressive severity of disease (*67*). Twin studies have also documented the inheritance of telomere length (*68*).

Analysis of chromosome end–specific telomere lengths across 147 individuals showed that specific telomeres tend to be the longest or shortest, supporting a previous study using qFISH on 10 individuals (*20*). Cord blood also showed that 17p, 20q, and 12p were among the shortest and 4q, 12q, and 3p were among the longest ends, suggesting that telomere length

differences present at birth are maintained over decades. This establishment of chromosome end–specific telomere length equilibria at birth (*46*) and maintenance of ranking patterns after birth suggests that increased cell division with age, not life history (*69*), is the major driver of telomere shortening. The similarity of our data to Martens *et al.* qFISH analysis is notable, and our method will enable future studies to explore the biological significance of this finding. We did not prospectively choose our samples to be representative of the diversity of the human population but rather to span a wide age range. However, future studies should be powered to examine whether certain chromosome ends are consistently the shortest or longest more broadly in a diverse human population.

Implications for human disease

Being able to accurately measure chromosome end–specific telomere length has important implications for understanding human disease. Telomere Profiling permits length determination at near-nucleotide resolution and can distinguish the length of specific chromosome ends. Telomere Profiling uses the accessible ONT MinION instrument, which can be used in-house in any research or clinical lab with very low start-up costs, allowing for broad access to accurate and reproducible telomere length determination. This provides the opportunity for prospective studies to develop clinical standards analogous to those for FlowFISH and may allow clinical length measurements in samples other than blood. In addition, having a highly reproducible assay that can be easily automated will enable experimental approaches to define previously unknown regulators of telomere length. The requirement of telomere elongation for immortalization of cancer cells has been known since 1990 (*28*, *70*, *71*). Sequence-level Telomere Profiling may enable development of new screening assays for telomere length modulation to develop new cancer drugs. Finally, the identification of conserved chromosome end–specific telomere lengths implies that as yet undiscovered biological mechanisms influence telomere length. Telomere Profiling will empower the field as a whole to dissect these mechanisms, leading to new discoveries in telomere biology.

REFERENCES AND NOTES

1. C. W. Greider, E. H. Blackburn, *Cell* **43**, 405–413 (1985).
2. M. Armanios, *Annu. Rev. Genomics Hum. Genet.* **10**, 45–61 (2009).
3. M. Armanios, *Annu. Rev. Genomics Hum. Genet.* **23**, 363–381 (2022).
4. S. Horn *et al.*, *Science* **339**, 959–961 (2013).
5. F. W. Huang *et al.*, *Science* **339**, 957–959 (2013).
6. M. T. Teixeira, M. Arneric, P. Sperisen, J. Lingner, *Cell* **117**, 323–335 (2004).
7. S. Marcand, E. Gilson, D. Shore, *Science* **275**, 986–990 (1997).
8. A. Smogorzewska *et al.*, *Mol. Cell. Biol.* **20**, 1659–1668 (2000).
9. E. H. Blackburn, S. S. Chiou, *Proc. Natl. Acad. Sci. U.S.A.* **78**, 2263–2267 (1981).
10. J. W. Szostak, E. H. Blackburn, *Cell* **29**, 245–255 (1982).
11. S. Marcand, D. Wotton, E. Gilson, D. Shore, *Ciba Found. Symp.* **211**, 76–93 (1997).
12. D. Wotton, D. Shore, *Genes Dev.* **11**, 748–760 (1997).
13. D. L. Levy, E. H. Blackburn, *Mol. Cell. Biol.* **24**, 10857–10867 (2004).
14. N. Rufer, W. Dragowska, G. Thornbury, E. Roosnek, P. M. Lansdorp, *Nat. Biotechnol.* **16**, 743–747 (1998).
15. G. Aubert, M. Hills, P. M. Lansdorp, *Mutat. Res.* **730**, 59–67 (2012).
16. J. K. Alder *et al.*, *Proc. Natl. Acad. Sci. U.S.A.* **115**, E2358–E2365 (2018).
17. M. Armanios, *J. Clin. Invest.* **123**, 996–1002 (2013).
18. P. M. Lansdorp *et al.*, *Hum. Mol. Genet.* **5**, 685–691 (1996).
19. J. M. Zijlmans *et al.*, *Proc. Natl. Acad. Sci. U.S.A.* **94**, 7423–7428 (1997).
20. U. M. Martens *et al.*, *Nat. Genet.* **18**, 76–80 (1998).
21. J. A. Londoño-Vallejo, H. DerSarkissian, L. Cazes, G. Thomas, *Nucleic Acids Res.* **29**, 3164–3171 (2001).
22. S. L. Sholes *et al.*, *Genome Res.* **32**, 616–628 (2022).
23. K. Grigorev *et al.*, *Genome Res.* **31**, 1269–1279 (2021).
24. C. Y. Tham *et al.*, *Nat. Commun.* **14**, 281 (2023).
25. D. Dubocanin *et al.*, bioRxiv 2022.05.09.491186 [Preprint] (2022); https://doi.org/10.1101/2022.05.09.491186.
26. P. Giesselmann *et al.*, *Nat. Biotechnol.* **37**, 1478–1481 (2019).
27. C. B. Harley, A. B. Futcher, C. W. Greider, *Nature* **345**, 458–460 (1990).
28. N. D. Hastie *et al.*, *Nature* **346**, 866–868 (1990).
29. H. Vaziri *et al.*, *Am. J. Hum. Genet.* **52**, 661–667 (1993).
30. G. Aubert, G. M. Baerlocher, I. Vulto, S. S. Poon, P. M. Lansdorp, *PLOS Genet.* **8**, e1002696 (2012).
31. A. Aviv, *J. Gerontol. A Biol. Sci. Med. Sci.* **63**, 979–983 (2008).
32. N. Rufer *et al.*, *J. Exp. Med.* **190**, 157–167 (1999).
33. U. M. Martens *et al.*, *Br. J. Haematol.* **119**, 810–818 (2002).
34. M. Y. Armanios *et al.*, *N. Engl. J. Med.* **356**, 1317–1326 (2007).
35. J. A. Van Ziffle, G. M. Baerlocher, P. M. Lansdorp, *Stem Cells* **21**, 654–660 (2003).
36. G. M. Baerlocher, P. M. Lansdorp, *Cytometry A* **55A**, 1–6 (2003).
37. J. K. Alder, M. Armanios, *Physiol. Rev.* **102**, 1703–1720 (2022).
38. K. Lakota *et al.*, *Ann. Rheum. Dis.* **78**, 1142–1144 (2019).
39. S. Garg *et al.*, *Nat. Biotechnol.* **39**, 309–312 (2021).
40. N. Stong *et al.*, *Genome Res.* **24**, 1039–1050 (2014).
41. H. Li, *Bioinformatics* **34**, 3094–3100 (2018).
42. H. Li, *Bioinformatics* **37**, 4572–4574 (2021).
43. K. T. Tan, M. K. Slevin, M. Meyerson, H. Li, *Genome Biol.* **23**, 180 (2022).
44. W. W. Liao *et al.*, *Nature* **617**, 312–324 (2023).
45. S. E. Antonarakis, *Genome Res.* **32**, 599–607 (2022).
46. J. Graakjaer *et al.*, *Aging Cell* **3**, 97–102 (2004).
47. M. T. Hemann, M. A. Strong, L.-Y. Hao, C. W. Greider, *Cell* **107**, 67–77 (2001).
48. F. d'Adda di Fagagna *et al.*, *Nature* **426**, 194–198 (2003).
49. S. Enomoto, L. Glowczewski, J. Berman, *Mol. Biol. Cell* **13**, 2626–2638 (2002).
50. A. S. IJpma, C. W. Greider, *Mol. Biol. Cell* **14**, 987–1001 (2003).
51. E. J. McNally, P. J. Luncsford, M. Armanios, *J. Clin. Invest.* **129**, 3474–3481 (2019).
52. A. Smogorzewska, T. de Lange, *Annu. Rev. Biochem.* **73**, 177–208 (2004).
53. D. Shore, A. Bianchi, *EMBO J.* **28**, 2309–2322 (2009).
54. A. J. Lustig, *Nat. Rev. Genet.* **4**, 916–923 (2003).
55. M. Zimmermann, T. Kibe, S. Kabir, T. de Lange, *Genes Dev.* **28**, 2477–2491 (2014).
56. M. Paschini *et al.*, bioRxiv 2020.08.05.237172 [Preprint] (2020); https://doi.org/10.1101/2020.08.05.237172.
57. M. Arnerić, J. Lingner, *EMBO Rep.* **8**, 1080–1085 (2007).
58. W. R. A. Brown *et al.*, *Cell* **63**, 119–132 (1990).
59. S. G. Nergadze *et al.*, *RNA* **15**, 2186–2194 (2009).
60. Z. Deng *et al.*, *EMBO J.* **31**, 4165–4178 (2012).
61. M. Feretzaki, P. Renck Nunes, J. Lingner, *RNA* **25**, 1470–1480 (2019).
62. M. Achrem, I. Szućko, A. Kalinka, *Comp. Cytogenet.* **14**, 265–311 (2020).
63. S. Toubiana, S. Selig, *Curr. Opin. Genet. Dev.* **60**, 9–16 (2020).
64. S. Gonzalo *et al.*, *Nat. Cell Biol.* **8**, 416–424 (2006).
65. N. Arnoult *et al.*, *PLOS Genet.* **6**, e1000920 (2010).
66. M. Armanios, E. H. Blackburn, *Nat. Rev. Genet.* **13**, 693–704 (2012).
67. L. Y. Hao *et al.*, *Cell* **123**, 1121–1131 (2005).
68. P. E. Slagboom, S. Droog, D. I. Boomsma, *Am. J. Hum. Genet.* **55**, 876–882 (1994).
69. Q. A. Conklin, A. D. Crosswell, C. D. Saron, E. S. Epel, *Curr. Opin. Psychol.* **28**, 92–101 (2019).
70. C. W. Greider, *BioEssays* **12**, 363–369 (1990).
71. T. de Lange *et al.*, *Mol. Cell. Biol.* **10**, 518–527 (1990).
72. K. Karimian *et al.*, Telomere dataset used for calculating bulk and chromosome specific telomere length, Dryad (2024); https://doi.org/10.5061/dryad.dz08kps5d.
73. A. Rechtsteiner, K. Karimian, C. W. Greider, Telomere Read Analysis, version 0.9, Zenodo (2024); https://doi.org/10.5281/zenodo.10895154.
74. R. Kahidi, K. Karimian, C. W. Greider, TeloBP/TeloNP: Initial Release, version 1.0.0, Zenodo (2024); https://doi.org/10.5281/zenodo.10826387.
75. R. Kahidi, K. Karimian, C. W. Greider, TeloPeakCounter: Initial Release, version 1.0.0, Zenodo (2024); https://doi.org/10.5281/zenodo.10892178.

ACKNOWLEDGMENTS

We thank R. Green for provision of laboratory space at Johns Hopkins University as well as discussions and B. Cormack and C. Gao for reviewing the manuscript. C. Connelly, J. Brunelle, and M. Strong provided experimental and logistical assistance. We thank M. Armanios and her lab for help in the early stages of assay development and L. Danilova for statistical analysis. We thank M. Paniagua for assistance with reagent procurement. **Funding:** This work was supported by National Institutes of Health grant R35CA209974 (C.W.G.), a Johns Hopkins Bloomberg Distinguished Professorship (C.W.G.), National Institutes of Health grant R01HL166265 (J.K.A. and J.F.M.), National Science Foundation Graduate Research Fellowship Program DGE-1746891 (K.K.), and National Institutes of Health grant T32GM007445 (K.K., S.S., and R.Ke.). **Author contributions:** Conceptualization: C.W.G., K.K., and S.S. Data curation: A.G., K.K., R.Ka., R.Ke., and A.R. Formal analysis: K.K., R.Ka., A.R., and S.S. Funding acquisition: C.W.G., H.L., J.K.A., and J.F.M. Investigation: A.G., V.H., K.K., and R.Ke. Methodology: C.W.G., V.H., K.K., R.Ka., R.Ke., A.R., and S.S. Project administration: C.W.G. Resources: J.K.A., C.W.G., J.F.M., and K.K. Software: K.K., R.Ka., H.L., A.R., and K.-T.T. Supervision: C.W.G. and H.L. Validation: C.W.G., A.G., K.K., R.Ka., A.R., and S.S. Visualization: J.K.A., K.K., R.Ka., and A.R. Writing – original draft: C.W.G. and K.K. Writing – review & editing: J.K.A., C.W.G., A.G., V.H., K.K., A.R., and S.S. **Competing interests:** C.W.G. and K.K. are inventors of US Patent WO 2024/050553 titled "Methods for telomere length measurement." All other authors declare that they have no competing interests. **Data and materials availability:** All data, code, and materials used in the analysis will be provided to any researcher to reproduce or extend this analysis. The HG002 cell line is available from Coriell under a material transfer agreement. IPF samples were part of the Breath-LT biorepository and accessed through a material transfer agreement with the University of Pittsburgh. All fastq telomere sequencing files generated in this study are available in Dryad (*72*). Given size limitations and human subject protections, fast5 electrical signal files will be made available upon request. The code for Telomere read analysis (*73*), TeloBP and TeloNP (*74*), and TeloPeakCounter (*75*) is available in Zenodo and at https://github.com/GreiderLab.

SUPPLEMENTARY MATERIALS

science.org/doi/10.1126/science.ado0431
Materials and Methods
Figs. S1 to S6
Tables S1 to S3
References
MDAR Reproducibility Checklist

Submitted 14 January 2024; accepted 30 March 2024
Published online 11 April 2024
10.1126/science.ado0431